Thesis for the Degree of Licentiate of Physics

Low Noise Frequency Combs and Their Use in Broadly Tunable Lasers and Optical Coherence Tomography

J. Connor Skehan

CHALMERS

Photonics Laboratory
Department of Microtechnology and Nanoscience - MC2
Chalmers University of Technology
Göteborg, Sweden, 2022

Low Noise Frequency Combs and Their Use in Broadly Tunable Lasers and Optical Coherence Tomography
J. Connor Skehan
Göteborg, December 2022

Chalmers University of Technology
Microtechnology and Nanoscience - MC2
Photonics Laboratory
SE-412 96 Göteborg, Sweden
Phone: +46 (0) 31 772 1000

ISSN 1652-0769
Technical Report MC2-447

Printed in Sweden by Reproservice, Chalmers University of Technology
Göteborg, Sweden, February 2022

Low Noise Frequency Combs and Their Use in Broadly Tunable Lasers and Optical Coherence Tomography

J. Connor Skehan
Photonics Laboratory
Department of Microtechnology and Nanoscience - MC2
Chalmers University of Technology

Abstract

Frequency combs revolutionized the world of laser physics by providing a link between the microwave and optical domains. Such a link allows for precise knowledge of any comb line's absolute average location, as well as the average spacing between any two comb lines.

Here, we exploit this knowledge for a variety of applications, and study the limits thereof. Combs from a variety of sources are studied, and in all cases, low noise and/or highly mutually coherent tones can be readily produced which are useful in a variety of contexts.

More specifically, the phase/frequency noise of comb tones is investigated, along with the mutual coherence between two comb lines. In addition, the relative intensity noise of a full comb spectra and of individual comb lines is also investigated.

The low phase/frequency noise of individual comb lines as produced in electro-optic and in normal dispersion photonic molecules is used for the generation of highly tunable and low noise laser sources, and the high mutual coherence and precise repetition rate of an anomalous dispersion microresonator combs is used for optical coherence tomography.

Keywords: optical frequency comb, comb noise, optical injection locking

Publications

This thesis is based on the work contained in the following papers:

[A] **J. Connor Skehan**, Corentin Naveau, Jochen Schröder, and Peter Andrekson
"Widely tunable, low linewidth, and highpower laser source using an electro-optic comb and injection-locked slave laser array",
Optics Express, vol. 29, no. 11, May 2021

[B] **J. Connor Skehan**, Oskar B. Helgason, Jochen Schröder, Victor Torres-Company, and Peter Andrekson
"Widely Tunable and Narrow Linewidth Laser Sourced based on Normal-Dispersion Frequency Combs and Optical Injection Locking",
submitted to *Conference on Lasers and Electro-Optics (CLEO)*, San Jose, USA, May 2022.

[C] Paul J. Marchand, Johann Riemensberger, **J. Connor Skehan**, Jia-Jung Ho, Martin H. P. Pfeiffer, Junqiu Liu, Christoph Hauger, Theo Lasser, Tobias J. Kippenberg
"Soliton microcomb based spectral domain optical coherence tomography",
Nature Communications, 12:427, 2021.

The following papers include previous publications which are not included as part of the thesis, but are listed to provide context regarding my experience and acedemic interests.

[D] **Connor Skehan**, Bin Ai, Steven R Larson, Keenan M Stone, William M Dennis, Yiping Zhao
"Plasmonic and SERS performances of compound nanohole arrays fabricated by shadow sphere lithography",
Nanotechnology, volume 29.9, 095301

[E] Mikhail Churaev, Simon Honl, Rui Ning Wang, Charles Mohl, Tianyi Liu, **J Connor Skehan**, Johann Riemensberger, Daniele Caimi, Junqiu Liu, Paul Seidler, Tobias J Kippenberg
"Hybrid Si3N4-LiNbO3 integrated platform for electro-optic conversion",
CLEO : Science and Innovations, May 2020, STh1F.3

[F] Jeff Chiles, Nima Nader, Eric J Stanton, Daniel Herman, Galan Moody, Jiangang Zhu, **J Connor Skehan**, Biswarup Guha, Abijith Kowligy, Juliet T Gopinath, Kartik Srinivasan, Scott A Diddams, Ian Coddington, Nathan R Newbury, Jeffrey M Shainline, Sae Woo Nam, Richard P Mirin
"Multifunctional integrated photonics in the mid-infrared with suspended AlGaAs on silicon",
Optica, Volume 6.9, 1246-1254

[G] Alexey Tikan, Johann Riemensberger, Kenichi Komagata, Simon Hönl, Mikhail Churaev, **Connor Skehan**, Hairun Guo, Rui Ning Wang, Junqiu Liu, Paul Seidler, Tobias J Kippenberg
"Emergent nonlinear phenomena in a driven dissipative photonic dimer",
Nature Physics, Volume 17.5, 604-610

[H] Hao Tian, Junqiu Liu, Bin Dong, **J Connor Skehan**, Michael Zervas, Tobias J Kippenberg, Sunil A Bhave
"Hybrid integrated photonics using bulk acoustic resonators",
Nature communications, Volume 11.1, 1-8

[I] Hao Tian, Junqiu Liu, **Connor Skehan**, Anat Siddharth, Tobias J Kippenberg, Sunil A Bhave
"A Nitride Ring Isolator",
Cleo : Science and Innovations, STu4O.2

[J] A Tikan, J Riemensberger, K Komagata, S Hönl, M Churaev, **C Skehan**, H Guo, RN Wang, J Liu, P Seidler, TJ Kippenberg "Dissipative Kerr solitons in a photonic dimer", *2020 Conference on Lasers and Electro-Optics (CLEO), Pages 1-2*

Contents

Acknowledgement

I'd first like to acknowledge my friends, family, and loved ones, whose support is truly invaluable. Without them, no part of my life could be possible.

I'd next like to my colleagues for their support and dedication, and for their role in continuing to pass down knowledge from one academic to another - as has been the tradition for many hundreds of years. To continue this transfer of knowledge is essential for any high functioning human society, as it allows us to stand on the shoulders of giants.

J. Connor Skehan
Göteborg, December 2022

On the planet Earth, man had always assumed that he was more intelligent than dolphins because he had achieved so much - the wheel, New York, wars and so on - whilst all the dolphins had ever done was muck about in the water having a good time. But conversely, the dolphins had always believed they were far more intelligent than man - for precisely the same reasons.

Douglas Adams
The Hitchhiker's Guide to the Galaxy

Acronyms

AOM	acousto-optic modulator
ASE	amplified spontaneous emission
CEO	carrier-envelope offset
CW	continuous wave
DFB	distributed feedback
ECDL	external cavity diode laser
EDFA	erbium-doped fiber amplifier
EM	electro-magnetic
EO	electro-optic
ESA	electric spectrum analyzer
FBG	fiber Bragg grating
FSR	free spectral range
FT	Fourier transform
FWHM	full-width half-max
LIDAR	light detection and ranging
LLE	Lugiato-Lefever equation
MI	modulation instability
MZI	Mach Zehnder interferometer
NLSE	nonlinear Schrödinger equation
NF	noise figure
OCT	optical coherence tomography
OFC	optical frequency comb
OIL	optical injection locking
P/FN	phase / frequency noise

PSA	phase sensitive amplification
PSD	power spectral density
RF	radio frequency
RIN	relative intensity noise
SCG	supercontinuum generation
SMSR	side-mode suppression ratio
SNR	signal to noise ratio

CHAPTER 1

Introduction

1.1 Overview

This thesis focuses primarily on the noise properties of optical frequency combs, and its individual tones. It will also cover various applications which take advantage of comb lines with low noise, and of combs which have a high mutual coherence between comb lines.

Amplitude and phase/frequency noise of comb tones is investigated and exploited for a variety of applications, including the production of highly tunable and low-noise lasers, and the high degree of mutual coherence between comb lines is important in, for example, optical coherence tomography.

1.2 Contents of the Thesis

This thesis consists of a short overview and introduction, followed by a discussion on frequency combs, and an analysis of the two types of combs seen in this work, namely electro-optic (EO) and microresonator frequency combs.

Next there is a brief discussion on optical noise in single frequency sources, including relative intensity noise (RIN) and phase / frequency noise (P/FN), as well as a discussion on the mutual coherence between two arbitrarily chosen comb lines. This is followed by a discussion on the

noise due to optical amplification and how to minimize this via optical injection locking (OIL), and a final discussion on optical frequency comb (OFC)s and their particular noise properties.

Finally, a brief commentary regarding the future outlook for this research will be presented, followed by a summary of the papers herein. Lastly, the actual papers relevant to the work are attached.

1.3 History, Relevance & Importance

Lasers are a mature technology which originated in the 1950's [1], and which have a plethora of implementations and applications which have changed the way we live our lives. These range from everyday items we use ourselves like barcode scanners [2] and Blu-Ray disk readers [3], to common activities we take for granted such as long haul optical communications [4], and even to highly specialized applications such as the detection of gravitational waves and the monitoring of nuclear fission reactors [5–7].

For this thesis, the primary laser source used is an OFC [8], a relatively recent advancement in the field of laser physics which came about near the turn of the 21st century. In general, a frequency comb can be thought of as a series of equally spaced non-zero amplitude modes in the frequency domain. If the comb lines are mutually coherent, the result in the time domain is a sequence of pulses. However, if the comb lines are not mutually coherent, the result in the time domain is a noisy superposition of uncorrelated optical modes.

While frequency combs were originally invented to probe various constants of the hydrogen atom to validate or invalidate fundamental theories of physics [8], they have since found a wide range of applications, including the generation of optical clocks [9,10], timing and synchronization of clock networks [11,12], distance ranging and LIDAR [13,14], dual-comb spectroscopy [15], production of low noise microwave signals [16], and more [17].

Since their conception, a variety of comb sources have also been developed. These include mode locked fiber frequency combs [18], photonic chip based microcombs [19] and monolithic crystalline combs [20] (both of which are types of Kerr combs), and EO combs [21], among others.

Each OFC application has its own requirements in terms of spectral bandwidth, central frequency, noise properties, power, etc. that is best fulfilled by a particular type of comb.

Low noise and low repetition rate (on the order of 100 MHz) combs such as fiber frequency combs are used in timing synchronization and optical clocks [10], as well as supercontinuum generation (SCG) without the need for pulse compression [22], but were first used for spectroscopy, where the low repetition rate and high stability means that many comb lines might cover a single absorption line of an atom, allowing for precise measurement of single and multi-species gaseous samples [8]. One common application of such combs is in dual comb spectroscopy [23], whereby two combs of different repetition rates act together to produce a coherent multiheterodyne interferometer.

Other applications such as LIDAR (LIght Detection And Ranging, an optical analog of RADAR) [24], low noise microwave generation [25], and optical communications require larger comb mode spacing (corresponding to a higher repetition rate) [26]. To that end, monolithic crystalline combs, integrated photonic microcombs, and EO combs are often used, where repetition rates can span anywhere from a few GHz up to the THz regime.

Combs have a huge range of applications themselves, but the tones of a frequency comb are also useful in their own right. The individual lines of the comb may be selected using a fiber Bragg grating (FBG), bandpass filter, etc., then used for their own purpose. Two tones might beat against one another to produce a high frequency tone beyond the FSR of the comb, or the comb line might be used as an optical reference.

This thesis, consisting of 3 appended papers, is focused on two distinct applications of OFCs. The first of these is the production of low noise and highly tunable laser sources [27–31] (for their eventual use in-house regarding phase sensitive amplification (PSA)), and the second is in optical coherence tomography (OCT), an imaging technique capable of resolving scattering media in all three dimensions [32, 33].

PSAs [34] are an optical amplification scheme based on nonlinear optical processes in a dielectic medium, and are of importance because they are able to break the classical noise figure (NF) limit of 3 dB. In such a device, some combination of 4 waves are present (including the possibility of degenerate electro magnetic (EM) fields), 2 of which act as pumps (and a source of power), and two of which act as the so called signal and idler (which are amplified). To ensure proper operation, the signal and idler must be properly spaced from the pumps(s), and their relative phase differences must be optimized for maximum gain according to material parameters such as dispersion, and nonlinear refractive

index. Typically, a so-called "copier" scheme is used before the PSA to nonlinearly produce the conjugate idler, which makes the amplification independent of modulation format. Alternatively though, one could use a precisely placed conjugate of the signal, and (in the case of optical communication systems) simply encode conjugate data on it. For this, a highly precise and broadly tunable, low noise source is required.

PSAs have their own applications, but being able to produce a highly tunable and low noise source is important for a huge range of applications, including spectroscopy [35], interferometry [36], and metrology [37], as well as in general communications [38], for optical tweezers [39], LIDAR [40–42], GPS systems [43], and for driving other lasers such as Raman [44–46] and Brillouin lasers [47–49]. State of the art and commercially available technology tends to rely on fiber lasers which are not particularly tunable, or external cavity diode laser (ECDL)s which can have low noise and be extremely tunable, but are costly, have a large footprint, and are difficult to deploy in the field.

Combs also have a use in optical coherence tomography, a reflective imaging technique in which the output of a spectrally resolved Michelson interferometer is used to recover backscattered light from a thin sample. The source beam is split into two arms at the input of the interferometer, one of which is held static as a reference path, while the other is allowed to scan over some shallow tissue sample and recover backscattered light. The resulting interference pattern can be Fourier transformed to produce a depth map of the sample. By scanning over the sample, a fully three dimensional scan can be produced which is useful in a wide variety of contexts, mostly medical. In the case of frequency comb OCT [50–52], intermediate frequencies between tones can be ignored and thus reduce system noise, but in the special case when using a coherent comb in the form of a pulse, noise on each line is shared and thus spectral fluctuations do not degrade the final image. In other words, the low noise floor between comb lines reduces speckle in the final image, and the high degree of correlation between tones reduces systematic errors.

CHAPTER 2

Optical Frequency Combs

Optical frequency combs are a special case of lasers which come in a variety of forms [17, 53–60], but in all cases be described by a series of distinct, non-zero amplitude optical modes in the frequency domain which have equal frequency spacing, and some shared offset frequency from zero. We can write the optical amplitude spectrum as follows :

$$\tilde{A}(\omega) = \sum_{m=0}^{+\infty} A_m e^{i\omega_m t} \tag{2.1}$$

where $A(\omega)$ is the amplitude spectrum of the wave, and A_m is the amplitude of the m^{th} mode.

If we assume the lines to be mutually coherent, a series of pulses is formed in the time domain, as seen in figure 2.1. In this case, ω_r can be thought of as the pulse's repetition rate, and ω_0 can be thought of as the carrier-envelope offset frequency of the pulse, and is related to the instantaneous carrier envelope offset (CEO) offset, ϕ_{CEO}, between any two subsequent pulses by

$$\omega_0 = \frac{1}{2\pi}\frac{d}{dt}\phi_{CEO}(t) \tag{2.2}$$

Ignoring the instantaneous phase of individual comb lines in the time domain, we write this in the time domain as :

$$E(t) = \sum_{m=0}^{+\infty} A_m e^{i\omega_m t} \tag{2.3}$$

Such a pulse can be seen in both the time and frequency domains in figure 2.1, which serves to provide an intuitive understanding of the link between the time and frequency domains via the Fourier transform (FT). The frequency spacing between comb lines is directly related to the temporal spacing between pulses, and the shared offset of comb lines from zero in the frequency domain is directly related to the CEO frequency of phase offset.

2.1 Electro-Optic Combs

An EO comb is one of many types of frequency combs, and is created by passing a seed laser through some number of optical modulators in order to produce a series of equally spaced and cascaded modulation side-bands. Here, the comb's frequency spacing is directly determined by the modulation frequency (and thus the driving radio frequency (RF) signal), and the width of the comb is given by the strength of phase modulation.

Because the frequency line spacing (and corresponding repetition rate) is given by the RF clock which drives the modulation, ultra-high repetition rate (> 100 GHz) EO combs are impossible given the lack of ultra-high repetition rate RF driving signals / modulators. Moreover, expensive and lossy optical modulators, powered by energy-expensive amplifiers are required. Nevertheless, EO combs are robust, easy to operate, and are well described by linear functions, as shown below. All of which make them of interest in both scientific and practical applications.

If we write the seed laser in terms of the classic wave equation as follows [21],

$$A(t) = A_0 e^{i\omega_c t} \tag{2.4}$$

where A_0 is the wave amplitude, and ω_c is the carrier frequency, then we can phase modulate the wave with some driving field to find

$$\begin{aligned} A(t) &= A_0 e^{i\omega_c t} e^{iKV_0 \ \sin(\omega_m t)} \\ &= A_0 e^{i\omega_c t} e^{i\Delta\Phi} \end{aligned} \tag{2.5}$$

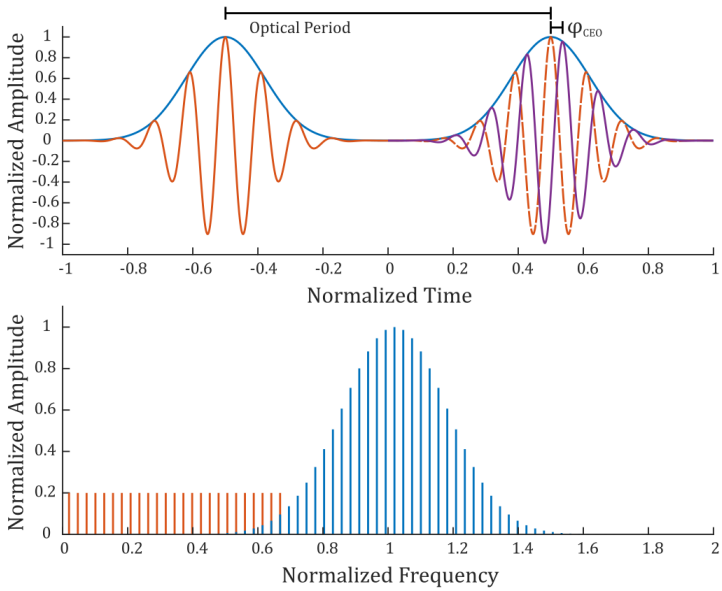

Figure 2.1: Top : two chirpless Gaussian pulses in succession, separated in the time domain by some period. Here, the dashed line indicates a copy of the first pulse which is superimposed on the second, to give a better indication of what is meant by the carrier envelop offset phase difference acquired between successive pulses. Bottom : a Gaussian frequency comb in blue, with spacing between optical modes equal to the comb's repetition rate. The offset frequency shared by all optical tones is equal to the frequency of carrier envelope offset overlap, as indicated by the lowest frequency orange line which corresponds to the $m = 0$ tone. Orange tones are not real, and are only given to highlight the frequency meaning of the CEO offset frequency.

where K is the phase modulation index, V_0 is the amplitude of the modulating signal, ω_m is the modulation frequency, $\Delta\Phi = KV(t)$ is the phase shift due to modulation, and $V(t) = V_0 \sin(\omega_m t)$.

Next, we if take the FT, we find that

$$\tilde{A}(\omega) = A_0 \int_{-\infty}^{+\infty} e^{i\Delta\Phi} e^{-i(\omega+\omega_c)t} dt \tag{2.6}$$

where we keep in mind that $\Delta\Phi = KV(t)$ is a function of t while integrating.

Next, we expand the plane wave as a series of cylindrical waves (i.e. the Jacobi-Anger expansion), and write

$$\begin{aligned} \tilde{A}(\omega) &= A_0 \int_{-\infty}^{+\infty} \left(\sum_{n=-\infty}^{+\infty} J_n(KV_0) e^{-i(\omega+\omega_c+n\omega_m)t} \right) dt \\ &= A_0 \sum_{-\infty}^{+\infty} J_n(KV_0) \delta(\omega - n\omega_m - \omega_c) \end{aligned} \tag{2.7}$$

where J_n are Bessel functions of the 1^{st} kind, and act as the envelope function which defines a comb of frequencies $\omega = n\omega_m + \omega_c$.

Importantly, if we introduce a static phase noise, ϕ, which arises due to the voltage onto and within the RF modulation, we now write $V(t) = V_0 \sin(\omega_m t + \phi)$, such that $\tilde{A}(\omega)$ becomes

$$\tilde{A}(\omega) = A_0 \sum_{-\infty}^{+\infty} J_n(KV_0) e^{in\phi} \delta(\omega - n\omega_m - \omega_c) \tag{2.8}$$

and we see that the phase noise due to due the voltage controlled oscillator (VCO), which drives $V(t)$, grows linearly with mode number n from the pump. This of course corresponds to a linear growth in phase noise and therefore linewidth as you move away from the center frequency.

We also notice that the end result of a single phase modulator is a superposition of a large number of Bessel functions. The amplitude difference between various comb lines varies considerably across the comb's bandwidth due to the complicated superposition of these Bessel functions. To compensate for this, a phase matched amplitude modulator is often placed after the phase modulator(s), in order to produce a smooth envelope (although not necessarily a flat-top envelope).

Figure 2.2 shows a simulated EO comb made via 2 phase modulators and 1 amplitude modulator, with a fixed phase relationship to ensure a maximum spectral bandwidth and a flat-top comb. The specific parameters of the simulation are such that the central frequency is set to 200 THz ($\sim$ 1500 nm), the driving RF field is set to 24.8 GHz, both the laser and modulation frequencies are given white and pink noise, and the phase modulation index, K, for both phase modulators is 3.375 V^{-1}, while the amplitude modulation index is set to 0.9, where the amplitude modulation index is defined as by the strong modulation amplitude divided by the amplitude of the unmodulated signal. Here, the noise on the pump laser dominates the accumulated noise from modulation, such that the noise floor of the simulated spectra is largely flat (such that the side-mode supression ratio (SMSR) of tones as compard to the noise floor is nearly equal for all modes)

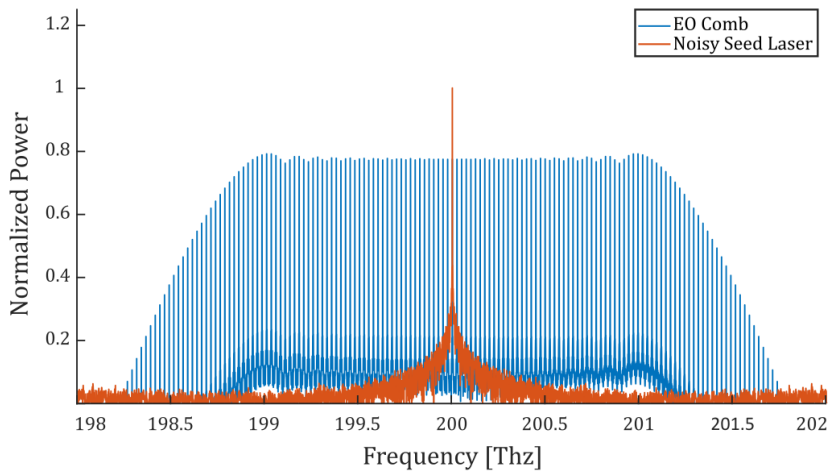

Figure 2.2: An EO comb simulated via the modulation of a noisy seed laser with an noisy RF tone. Here, two phase modulators and one amplitude modulator is used. The RF driving field is set to 24.8 Ghz such that it coincides with a multiple of the simulation's sampling frequency. K is set to 3.375 V^{-1} and the amplitude modulation index is set to 0.9.

2.2 Microresonator Combs

Photonic chip microresonator combs fall under the broader category of Kerr combs [53], named for their reliance on 3rd order optical nonlinearities to produce a series of equally spaced optical tones. This is possible thanks to the build up of light in high quality factor optical cavities.

In general, as seen in figure 2.3, the process can be described by a high power source traveling through a waveguide which is coupled to some high quality-factor optical resonator, where the quality factor, Q, is defined as $Q = \omega_r/\Delta\omega$, where ω_r is the angular frequency of some resonant mode in question, and $\Delta\omega$ is its full-width half-max (FWHM) bandwidth. In the limit of high Q, this definition is equivalent to 2π times the energy stored in the resonator, divided by the energy dissipated per cycle. Thus, a high quality factor cavity may allow for substantial build up of light inside the cavity.

This build up of light is often strong enough to excite nonlinear processes inside of the cavity. Indeed, for certain values of input power relative the the waveguide's nonlinear threshold and driving frequency relative the the cavity's natural resonance, the resulting output is a set of nonlinearlly produced and equally spaced lines in the frequency domain (i.e. an OFC). In special cases (assuming anomalous dispersion) when the cavity's gain and loss is balanced, and the nonlinear and dispersive phase shifts are balanced, the output may be a series of solitonic pulses in the time domain, sitting atop a strong continuous wave (CW) background.

Mathematically, the process can be thought of as a damped and driven version of the nonlinear Schrodinger equation (NLSE), which is written in dimensionless form as follows, in a form known as the dimensionless Lugiato Lefever equation (LLE):

$$\frac{\partial\Psi}{\partial T} = -(1 - i\xi_0)\Psi + \frac{i}{2}\frac{\partial^2\Psi}{\partial\Theta^2} + i|\Psi|^2\Psi + f \tag{2.9}$$

where $\Psi = \sqrt{\frac{2g_0}{\kappa}}A$ is the primary field,

$T = \frac{\kappa}{2}t$ represents slow time, which describes the wave's evolution after

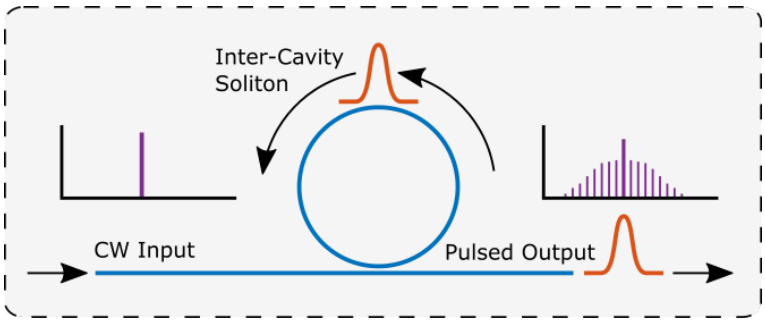

Figure 2.3: A high power continuous wave laser is injected into a wave guide which is coupled to a high Q-factor optical resonator. In the special case when optical gain and loss of the cavity are balanced, and nonlinear phase shift and dispersion are balanced, an optical soliton may form in the cavity, residing on top of a CW background. In this case, a highly coherent train of pulses is formed in the time domain, which corresponds to a frequency comb in the spectral domain.

each trip around the cavity

$\xi_0 = \frac{2}{\kappa}(\omega_p - \omega_r)$ is the cavity detuning,

$\Theta = \sqrt{\frac{\kappa}{2D_2}}\phi$ is the dispersion normalized angular position,

$f = \sqrt{\frac{P_{\text{in}}}{P_{\text{threshold}}}}$ is the pump power relative to the threshold power

$g_0 = \frac{\hbar\omega_0^2 c n_2}{n_g^2 V_{\text{eff}}}$ is the per photon nonlinear phase shift,

$\kappa = \kappa_{\text{intrinsic}} + \kappa_{\text{extrinsic}}$ is the inverse photon lifetime inside the cavity,

$P_{\text{threshold}} = \frac{\kappa^3}{8 g_0 \kappa_{\text{extrinsic}}}$ is the threshold power for modulation instability

A is the field amplitude normalized to photon count,
ω_p is the pump frequency,
ω_r is the cold resonance frequency,
D_2 is the walk-off from resonance due to 2^{nd} order dispersion, and
ϕ is the angular position in the cavity.
n and n_g are the regular and group indices of refraction, respectively
v_{eff} is the effective mode volume

The LLE is normally solved by dividing the equation into its linear ($\hat{D}$)

and nonlinear ($\hat{N}$) components [61], choosing an appropriate step size in time, and solving the two components separately, in a nearly identical manner to how one would normally solve the undamped and unpumped NLSE. Of course, higher order dispersive terms and various other nonlinear effects such as the Raman effect could be considered as well.

Importantly from the normalized and dimensionless LLE, we see than when given the resonator's dispersion profile, linewidth, and nonlinearity, the behavior of the system relies on only two parameters : the normalized detuning and normalized power.

When these two parameters are properly tuned relative to the given material parameters, the result is the generation of various cascaded four wave mixing (Kerr) modes in the frequency domain. Within this regime there are a large variety of still-being-explored states [62], such as the noisy, fully developed modulation instability (MI) state [63] which lacks mutual coherence between the comb lines, the multi and single soliton states (formed via an delicate balance between gain and loss on one hand, and phase shifts due to dispersion and nonlinearity on the other) [64,65], as well as more exotic states such as soliton crystals [66–68], breather solitons [69, 70], and more.

In general, the dispersion of the waveguide or material in which the soliton forms determines its spectral envelope [71], given that the process relies on unequally spaced allowable modes inside the cavity (whose position is determined by the material dispersion) and equally spaced non-zero amplitude optical modes as formed via nonlinear processes. Dispersive walk off of the cavity relative to the equally spaced modes therefore limits the optical bandwidth of the comb.

In [Paper C], we use a single-cavity anomalous dispersion Kerr microcomb to produce both fully developed MI states, as well as a single-soliton state in the cavity, and for this, the above equations work well. In [Paper B], however, we use a normal dispersion dual ring resonator system [72, 73]. Here, two LLEs should be constructed with mismatched free spectral range (FSR), and a coupling term should be added to each which allows for power transfer between the two cavities. In this case, a so-called photonic molecule is formed, where the second cavity acts to produce localized anomalous dispersion which can seed the process of side-band production in order to create a fully developed coherent comb state.

CHAPTER 3

Laser Noise

Noise is present in nearly all physical systems, and in lasers it comes in a variety of different forms depending on the particular kind of laser in question. In single-frequency [74, 75], CW lasers, there is only amplitude and phase/frequency noise which is native to the laser itself. In a system which lases at multiple modes simultaneously however, there also exists mode-beating and mode-partition noise which represent the intermodal interference and the random power transfer between modes, respectively. In pulsed lasers, there is also noise related to the repetition rate of the source (i.e. timing jitter), as well as the relative phase between the carrier and envelope waves.

Of course, noise can originate from many sources, but generally we can say that there are at least two sources common to nearly all lasers. Quantum noise, which refers to incoherent spontaneous emission in the gain medium (and often sets the lower limit for system performance), and technical noise, which refers to excess noise which comes from the environment such as the control electronics, vibrations, changes in temperature, etc.

3.1 Relative Intensity Noise

In all lasers, there is some degree of variation in the output power of the source, which, when normalized to the average output power, is called

RIN [76]. This manifests itself as noise on the A(t) component of the the optical wave equation for a single-frequency laser, i.e.

$$A(t) = [A_0 + \Delta A(t)] \cdot e^{i\omega_c t + \Delta\phi(t)} \tag{3.1}$$

Traditionally, the RIN of a laser source is measured as a function of frequency. The resulting power spectral density (PSD) measurement is given in units dBc/Hz (decibels under the carrier per Hertz) and communicates information about whether intensity fluctuations are rapid (such that they might be averaged way by a slow photodetector), slow (such that they might not matter for short detection periods), or present in large amounts only at a few select frequencies (such that a notch filter might fix the problem).

The signal to noise ratio (SNR) of a laser signal can be defined by the RIN, such that

$$\text{SNR} = \int_0^{\Delta f} \text{RIN}(f) df \tag{3.2}$$

where Δf is the receiver bandwidth.

Importantly, RIN can come from a variety of sources, both internal and external. For instance, in a fiber laser, RIN might be transfered from the pump onto the final output beam, but might also come from amplified spontaneous emission (ASE) inside the gain medium. Alternatively, RIN could come from technical noise stemming from thermal fluctuations, relaxation oscillations, etc.

To some extent, RIN in a single frequency laser can be mitigated. For instance, feedback loops on the control systems, temperature, etc. can mitigate and reduce technical noise. Alternatively, an intensity modulator such as an Mach-Zehnder interferometer (MZI) [77] or acousto-optic modulator (AOM) [78] could be used in either feedback or feedforward schemes.

RIN is fairly easy to measure directly [79], as the measurement scheme is simple and only consists of the beam, a single photodiode, and electronic spectrum analyzer.

3.2 Shot Noise

Shot noise is a type of laser amplitude noise which arises in photodetection due to the quantized nature of photons. It can be understood by viewing the optical field as a series of small, individual packets of

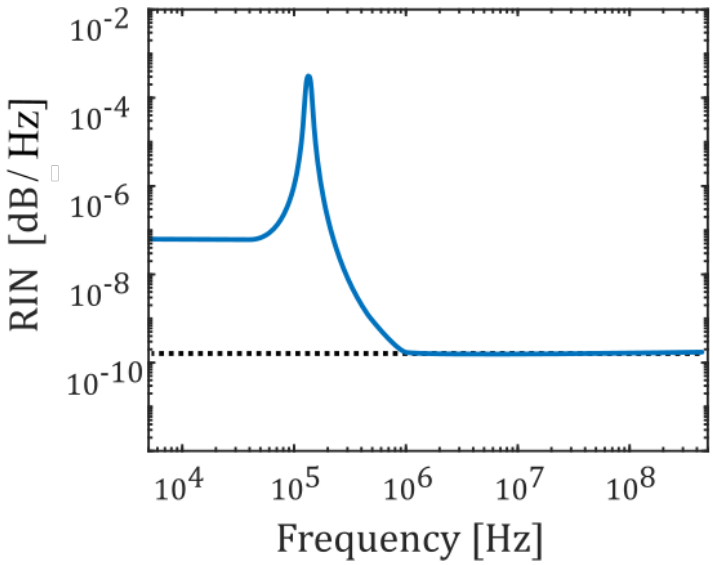

Figure 3.1: A typical, although idealized, RIN PSD which consists of a typical peak of some types of lasers which corresponds to relaxation oscillations, and white (Lorentzian) noise. The shot noise limit is given by the dashed black line.

energy which must therefore occur at the detector at random discrete time instances, instead of as a continuous flow. In this case, the single sided PSD of relative intensity noise is given by

$$S(f) = 2\hbar\nu\frac{1}{\bar{P}} \tag{3.3}$$

where $\hbar\nu$ is equal to the photon energy, and $\bar{P}$ is the average optical power.

Here, it can be seen that shot noise corresponds to white noise, and that by increasing the power, we reduce the shot noise of relative intensity noise.

A typical RIN spectrum might look like the PSD in figure 3.1, which includes typical noise contributions like the relaxation oscillation peak (which arise from oscillations corresponding to the return-to-normal state of certain types of lasers after being perturbed), and shot noise.

3.3 Phase & Frequency Noise

Phase and frequency noise are intricately connected. Indeed, the instantaneous frequency of a laser, ν is directly given by the derivative of phase, as

$$\nu(t) = \frac{1}{2\pi}\frac{d\phi}{dt} \tag{3.4}$$

and the power spectral densities $S_x(f)$ of each are also directly related, as per

$$S_\nu(f) = f^2 S_\phi(f) \tag{3.5}$$

In the spectral domain, phase and frequency noise manifest as the broadening of the laser's spectral linewidth [80], and in some instances, it may be advantageous to quantify this broadening in the form of a single parameter called linewidth, which may or may not include the additional contributes due to RIN.

Originally, laser linewidth was defined by the Schalow-Townes aproximation [81], also called the fundamental linewidth, and refers to the case of minimum possible noise (quantum noise) [82, 83], as given by

$$\Delta\nu_L = \frac{R_{\text{decay}} - R_{\text{st}}}{R_{\text{decay}}}\Delta\nu_c \tag{3.6}$$

where R_{decay} represents the rate of photon decay in the cavity, R_{st} gives the rate of stimulated emission, $\Delta\nu_c = (2\pi\tau_c)^{-1}$ represents the FWHM Lorentzian linewidth of the passive resonator mode in which gain occurs, and where τ_c is the exponential time constant of photon decay.

This approximation assumes a purely Lorentzian spectral shape of the laser's line, which corresponds to a flat, white spectral profile of the frequency noise PSD. This is never the case in reality, where there is inevitably some 1/f noise (aka pink noise, flicker noise) which dominates at low frequencies, and which occurs in nearly all electronic devices as a result of resistance fluctuations transforming into current or voltage fluctuations, but may also arise from thermal fluctuations, or a variety of other sources. This 1/f noise corresponds to a Gausian spectral profile, and thus (ignoring all other components), any real laser's spectral line will look like some combination of a Gaussian and Lorentzian function. A typical composite frequency noise spectrum is seen in figure 3.2.

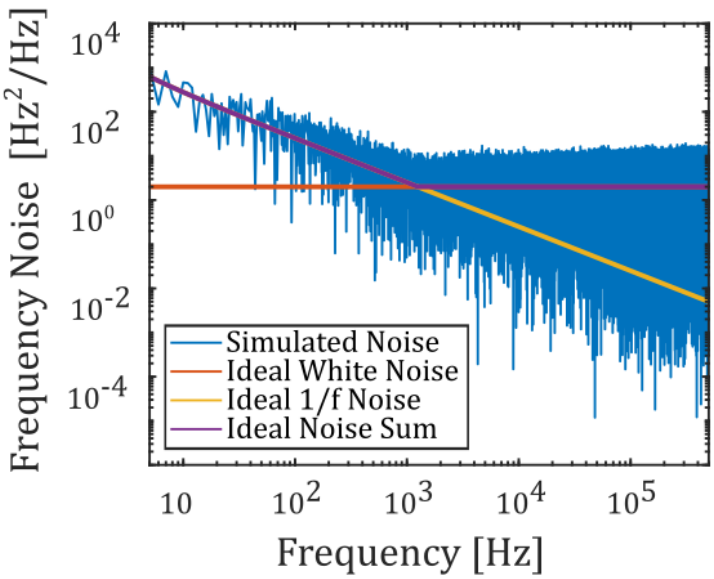

Figure 3.2: An idealized frequency noise PSD which consists of 1/f (Guassian) noise and white (Lorentzian) noise. At low frequencies, the Gaussian component dominates, while at high frequencies the Lorentzian component dominates.

To address this non-Lorentzian deviation from the ideal spectral line profile, there exist a variety of other definitions for linewidth which include higher order or noisy components which contribute to laser linewidth [84]. One such approach [85] is the intergrated linewidth definiton given below, where the linewidth is defined as the phase noise integral from infinity, down to whichever frequency, ν_{int}, corresponds to an area under the curve of $\frac{1}{\pi}$, such that

$$\int_{\nu_{int}}^{\infty} S_{\phi}(f)df = \frac{1}{\pi} \tag{3.7}$$

Competing approaches to address these inconsistencies include various fit methods and the beta line approach, for instance [80], which makes a strong assumption of the frequency noise PSD profile being either fully Gaussian or fully Lorenzian over some portion of the PSD, and therefore fail to address deviations from the Gaussian + Lorentzian assumed form (such that they fail under heavy technical noise). The integrated linewidth definition is more robust however, and is therefore preferable in many contexts, although it should be noted that it does tend to provide larger values of linewidth and is therefore often not provided.

On the other hand, when trying to investigate certain unavoidable and underlying properties of a laser, for instance, it is still often very useful to isolate your analysis from any technical or 1/f components, and focus interest solely on the lowest / white-noise limit of the system (i.e. the Lorentzian / Schalow-Townes aproximation), since this provides important information about properties such as fundamental quantum noise.

In figure 3.3, three different methods of recovering the linewidth are presented graphically to provide an intuitive explanation of the process. The integrated linewidth approach gives a value of approximately 1.5 kHz, while two fits to the same data are provided following the method outlined in [86] (which fits the data to white frequency noise in order to estimate the fundamental linewidth), the first of which includes excess noise and gives a value of approximately 710 Hz, and the second of which attempts to remove excess noise and provides a fundamental linewidth of approximately 120 Hz - more than 10 times less than the integrated linewidth and 5 times less than the fundamental linewidth as calculated including technical noise. It should be clear then, that any discussion of linewidth requires careful reading and a clear understanding of how the value was recovered, and what assumptions, if any, were made.

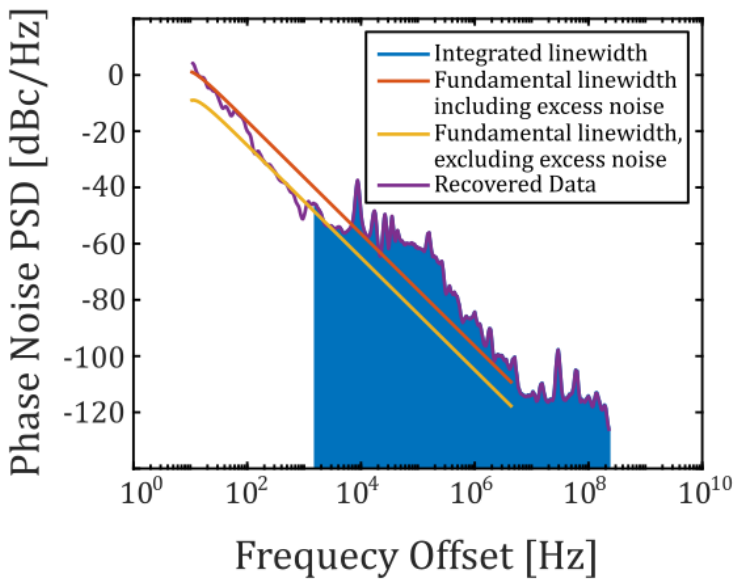

Figure 3.3: Different methods of fitting phase noise data leads to different recovered linewidths. The first fit type includes noise and gives a value of approximately 710 Hz, while the second tries to ignore additional noise and gives a recovered linewidth of 120 Hz. When using the integrated linewidth approach, a value of 1.5 kHz is recovered.

To some extent, phase noise, like RIN, may be controlled and possibly reduced in a rather straightforward manner, such as by using feedback loops onto the laser frequency controller, or by implementing feedback and feedforward schemes which rely on a phase modulator [87–90].

There are several approaches for the measurement of phase noise. The first class of measurement techniques rely on beating a noisy source against what is known to be an exceptionally low noise source such that any noise can be attributed to the noisy signal being measured. Similarly, there are a variety of techniques which rely on 3 sources in order to reduce the required assumptions and aide in the measurement of low noise lasers [91]. These measurement schemes are referred to as heterodyne measurements, given that the two distinct signals that are measured beat against one another.

The second class of measurements, called homodyne (or self - heterodyne) measurements begin by splitting the signal in two and passing one end through a delay line sufficiently long such that it is either fully or partially decoherent with its undelayed copy [92,93]. The two signals are then mixed together, and a beat note is measured. From this, one can measure the phase noise PSD directly, or measure the electronic spectra on an electric spectrum analyser (ESA) and extrapolate a linewidth measurement.

Self-heteroydyne approaches are valid, but extra care must be taken to select an appropriate delay length. For lasers with very low P/FN, impractical lengths of delay line might be needed for full decoherence of the two arms, which may introduce additional technical noise or loss such that the measurement is impossible. Instead, partially decoherent measurements are often required, which are only capable of measuring the noise within a particular bandwidth as set by the length of the delay line and the photodetector bandwidth. Importantly, in such measurements the beat signal will be near to baseband, and as such, should be frequency shifted using an AOM to avoid electronic measurement errors.

A simulated example of the electric spectrum for partially decoherent beams beating against one another is presented in figure 3.4. Here the linewidth of the laser is 212 Hz (a coherence time of 1.5×10^3 seconds), the delay line's length is set to 25 km, and any excess noise not related to the laser linewidth has been removed. The carrier frequency is set to 192 THz corresponding to a fiber index of refraction of 1.4682, and the AOM driving frequency is set to 25 MHz. A schematic outline of the optical setup for such a measurement can be found in [Papers A, B].

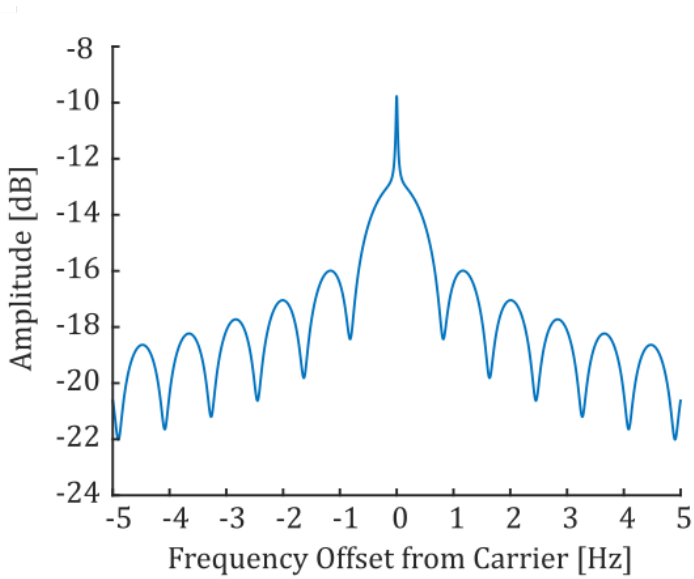

Figure 3.4: The electric spectrum of subcoherent beating, which might be recovered from the ESA in a delayed self heterodyne experiment. The original optical beam is split in two, then enters two arms of an interferometer. In the first arm, the light is amplitude modulated to shift the signal away from the DC limit, and in the other, the light enters a delay line which partially decoheres the two arms. The two beams are then mixed on a photodiode, and the resulting spectra is obtained.

In such a situation, the linewidth is given by a complex fit function, or can be estimated by measuring the relative strength between peaks and troughs of the spectrum's side lobes, as described below.

The spectrum of subcoherent beating in a delayed self-heteroydyne experiment is given as follows [94, 95]:

$$S(\omega,\tau) = \frac{A\tau_c}{1+\Delta\omega^2\tau_c^2}[[1 - [|\tau|e^{-|\tau|/\tau_c}\cos(\Delta\omega) + \frac{\sin(\Delta\omega)}{\Delta\omega}]] + \pi A e^{-|\tau|/\tau_c}\delta(\Delta\omega) \tag{3.8}$$

where $A = \frac{1}{2}P_o^2$, $\Delta\omega = \omega - \Omega$, Ω is the AOM driving frequency, τ is the delay time between arms, τ_c is the coherence time of the laser, and P_o is the optical power.

Given how difficult such a curve might be to fit, it is often easier to simply measure the phase/frequency noise PSD and directly integrate, although doing so is only truly valid from the inverse time delay, $\frac{1}{\tau}$, up to the bandwidth of the detector used. In the case where this integration does not reach the $\frac{1}{\pi}$ threshold, the curve is fit using white and pink noise as extrapolated from the given data set, or said to be under some threshhold linewidth.

Alternatively, one can make a few assumptions, as per [95, 96], and find that the amplitude difference between the first peak and trough for the subcoherent spectra, ΔS, is approximated by

$$\Delta S \approx 10\log_{10}\frac{16c}{9\pi nL\Delta\nu} \tag{3.9}$$

from which the linewidth can be derived, where n is the index of refraction and L is the length of the delay line.

3.4 Mutual Coherence

Although noise measurements of a single optical tone are important, it is often just as important to measure the degree to which two tones are correlated.

The mutual coherence of two optical tones is defined by

$$\gamma^2_{1,2}(f) = \frac{|S_{1,2}(f)|^2}{S_{1,1}(f)S_{2,2}(f)} \tag{3.10}$$

where $S_{1,2}$ is the cross spectral density of the signal, $S_{1,1}$ and $S_{2,2}$ are the power spectral density of the two signals in question, and where the cross spectral density and power spectral density are FTs of the cross-correlation and auto-correlations of the time domain signal, respectively.

Importantly, mutual coherence is a quantity which does not include the noise properties of each individual tone, and instead tries to quantify the amount of noise which is not common between the two measurements. For instance, if both tones suffer from technical noise due to a 1 MHz ground loop, this will not degrade the degree of mutual coherence between the two.

To measure the mutual coherence, two signals of equal power can be measured separately, and then analysed in post processing. Alternatively, the two signals may be directly beaten together and the an analysis of the beat note's noise may be considered along with the noise power spectral density of each individual beam.

Mutual coherence between two beams can be increased by locking two tones together. Here, one tone might be used as a reference frequency to which another beam is stabilized.

3.5 Low Noise Amplification via Optical Injection Locking

One particularly common source of noise in an optical system stems from the amplification of optical signals. In a traditional optical amplifier, amplification happens as a result of stimulated emission. However, spontaneous emission will also be present in such an amplifier, and the radiation created from this spontaneous emission will then act to seed further stimulated emission. The result is that ASE will always deteriorate the signal to noise ratio of an amplified signal by adding uncorrelated photons onto the optical field.

The total noise power from ASE in an amplifier (P_{ASE}) is given by

$$P_{ASE} = n_{sp}(G-1)hv \tag{3.11}$$

where n_{sp} is the spontaneous emission factor as given by $n_{sp} = \sigma_e N_2/(\sigma_e N_2 - \sigma_a N_1)$, G is the gain, and hv is the photon energy. σ_e and σ_a are the emission and absorption cross sections of the two level system with populations N_1 and N_2.

The amplifier's noise figure then, is given by

$$NF = \frac{SNR_{\text{in}}}{SNR_{\text{out}}} = 2n_{sp}\frac{G-1}{G} \tag{3.12}$$

which gives a limit of 2 (3dB) for classical optical amplification.

This additional noise comes in the form of broadband ASE noise underneath the amplified signal. To overcome this, an amplifier plus filter scheme is normally used, such that the optical SNR reduces to

$$SNR_o = \frac{P_{\text{in}}}{2P_{\text{ASE}}\Delta\nu} \tag{3.13}$$

where $\Delta\nu$ is the bandwidth of the optical filter used, and the factor of 2 stems from ASE at different polarizations when calculating the total ASE power.

In order to maximize the SNR_o, optical injection locking may be used [97, 98]. Here, instead of a traditional one way amplifier, amplification happens inside of a gain cavity (slave laser) whose oscillation, at sufficient

injected power and frequency detuning, will be forced to follow the same phase and frequency of the master (seed) laser. In doing so, a low, noisy or bulk laser may be forced to operate according to (what could be) a high quality, low noise laser. Furthermore, the total output power of the initially noisy laser may be substantially higher than the input, resulting in gain with minimal added noise. This is because in principle, the gain cavity is forced to oscillate at the same frequency as the input tone, and thus $\Delta\nu$ is minimized, and the optical SNR is maximized.

As will be seen below, such a locking behavior is only viable at particular offset frequencies and for particular input powers, however, and as such, a derivation of that behavior is required. In our theory of optical injection locking, we assume a single master laser to be working on a slave laser in such a way that the interaction is one sided (i.e. the slave laser does not act on the master laser).

This can be done by only slightly modifying the semi-classical laser rate equations by introducing a few additional terms which include the intensity of input light, the frequency of input light, and the phase of the input light.

The result of this analysis is the following rate equations [99, 100]

$$\frac{\delta A(t)}{\delta t} = \frac{1}{2}g[N(t) - N_{th}]A(t) + \kappa A_i \cos(\phi(t)) \tag{3.14}$$

$$\frac{\delta \phi(t)}{\delta t} = \frac{\alpha}{2}g[N(t) - N_{th}] - \kappa\frac{A_i}{A(t)}\sin(\phi(t)) - \Delta_\omega \tag{3.15}$$

$$\frac{\delta N(t)}{\delta t} = J - \gamma_N N(t) - A^2(t) \cdot \{\gamma_P + g[N(t) - N_{th}]\} \tag{3.16}$$

where $A(t)$ is the slowly varying varying field amplitude, g is the linear gain coefficient, $N(t)$ is the carrier number, N_{th} is the threshold carrier number for solitary operation of the slave laser, κ is the coupling coefficient, A_i is the injected field amplitude, $\phi(t)$ is the phase difference between the internal and injected fields, α is the linewidth enhancement factor, Δ_ω is the frequency difference between the internal and injected fields, J is the pump current normalized by electron charge, γ_N is the is the carrier decay rate, and γ_P is the photon decay rate.

Further, we can write the coupling coefficient, κ, as follows

$$\kappa = \frac{c}{2n_g L}\frac{1-R}{\sqrt{R}} = \frac{\omega_s}{2Q} \tag{3.17}$$

where c is the speed of light, n_g is the group refractive index of the laser cavity, L is the cavity length, R is the power reflectivity of the cavity mirror, and Q is the cavity's quality factor.

By solving for the steady state solutions of our rate equations, we find a locking bandwidth for which stable operation is possible. This is written as $\Delta\omega_{LB} = \Delta\omega_{max} - \Delta\omega_{min}$, where $\Delta\omega_{max}$ is the maximum of the asymmetric allowable detuning, and $\Delta\omega_{min}$ is the minimum of the asymmetric allowable detuning. After simplification, they are [99, 100]

$$\Delta\omega_{max} = \kappa\frac{\sqrt{P_i}}{\sqrt{P_o}} \tag{3.18}$$

$$\Delta\omega_{min} = -\kappa\sqrt{1+\alpha^2}\frac{\sqrt{P_i}}{\sqrt{P_o}} \tag{3.19}$$

with P_i and P_o representing the input and output powers of the slave laser, respectively, and their ratio is called the injection locking ratio, as plotted in figure 3.5.

Importantly, we find that $\Delta\omega_{LB}$ increases as the ratio of input power to (fixed) output power increases, and as κ increases. The first point implies that cavities are easier to lock when additional optical power is injected into the system, and the second implies that (since κ is inversely proportional to Q) a low quality factor cavity will be easier to lock. Of course, if one simply increases P_i, it should be easier for the injected power to overcome the cavity's ASE and begin lasing at the injected frequency, but in doing so, you increase the power requirements of the system and reduce the gain of the amplification scheme.

Under steady state conditions, there is a phase shift imparted on the output beam relative to the master is given by

$$\phi = \sin^{-1}\{\frac{\Delta\omega}{\Delta\omega_{min}}\} - \tan^{-1}(\alpha) \tag{3.20}$$

Thus, although the frequency of the output is stable, there is some phase difference between the injected and locked beams. Importantly, in the case that optical injection locking is achieved, any variation in the frequency detuning will not result in a shift in frequency, but instead in a phase shift. Of course, this also results in some additional phase/frequency noise on the system, given that the detunings themselves are subject to noise.

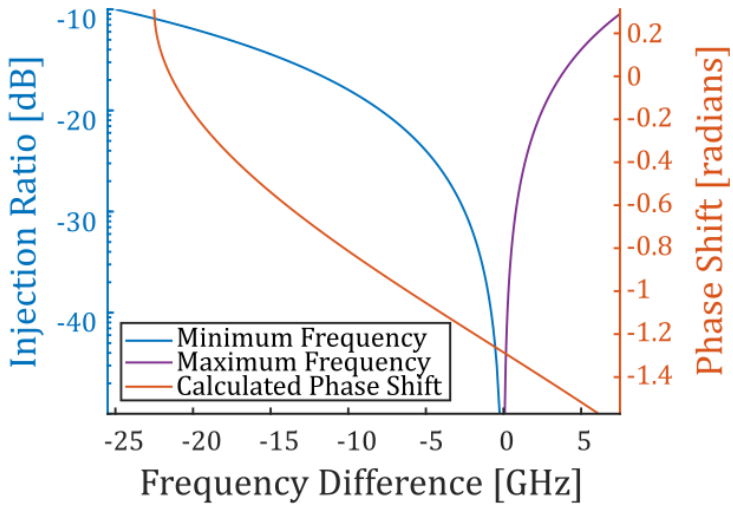

Figure 3.5: Locking conditions derived from the modified rate equations, equations 3.18 and 3.19. The mimimum offset frequency for locking is in blue, and the maximum is in purple. The phase shift curve in organge varies between the inverse cotangent of the linewidwth enhancement factor, α, for minimum detuning and $-\frac{\pi}{2}$ for maximum detuning. The phase shift curve given corresponds to an injection ratio of -17.5 dB (which corresponds itself to a maximum allowable detuning, $\Delta\omega$ of approximately 28 GHz). For all simulations, κ is set to 25×10^9, and α is set to 3.

3.6 Noise in Frequency Combs

Although it is customary and highly intuitive to understand an OFC's mode frequencies using just information about its repetition rate and CEO frequency, this model fails to accurately describe noise in OFCs. This is because the repetition rate and CEO noise are typically strongly correlated, given that f_{rep} noise necessarily impacts the comb's f_{CEO} [101, 102].

Instead, a common method for understanding the frequency location modes in an OFCs is the so-called elastic-tape model [103, 104], whereby we imagine some rubber band which is fixed to the frequency axis at one point, onto which the optical modes are placed. Some stretching force is then applied to both sides of the elastic tape, and the optical modes (now attached to the rubber band) move along in frequency space with this stretch. In this case, each source of noise might have it's own fixed point, and in an optical frequency comb, there are many sources of noise.

In general, this model provides some useful insights, and is aided by the following equation

$$f_{\text{fix}} = f_{\text{CEO}} \left(1 - \frac{\Delta f_{\text{CEO}} / f_{\text{CEO}}}{\Delta f_{\text{rep}} / f_{\text{rep}}} \right) \tag{3.21}$$

which allows us to find the fixed point frequency, f_{fix}, for any given fluctuation which changes either the CEO frequency or repetition rate.

Keeping in mind that the group delay determines the repetition rate of pulses, and the phase delay determines the phase progression of carrier waves, we note that when a change in the system modifies both the group and phase delays inside the cavity in nearly equal proportions, the CEO frequency will remain largely unchanged, but the repetition rate will be dramatically modified. This corresponds to (for instance) a change in the cavity length, and for a fixed point in the elastic tape model near the zero frequency point.

On the other hand, when a change in the system greatly modifies the phase delay, but not the repetition rate, the f_{CEO} will change drastically while the repetition does not, and the fixed point will be at some large nonzero value well past the comb's optical frequencies.

There are also many phenomena which produce effects somewhere in the space between these two extremes, such as thermal tuning which changes both the group and phase delay inside the cavity, but not in equal proportions. In such a situation, the fixed point of the elastic

tape model is at some large but non-zero frequency value, and makes stabilization difficult.

However, using knowledge of what drives these fluctuations in a particular comb, we can stabilize the device's f_{CEO} and f_{rep} both independently and simultaneously by using system perturbations which have different fixed points.

Of course, the elastic tape model is incomplete, and fails to capture anything beyond phase and frequency noise. In the case of optical communications, OCT, and LIDAR, we rely on a high ratio between the comb tooth power and the noise floor below it. That means we need not only a low linewidth for each optical mode relative to the mode spacing, but also a high SNR (and thus low RIN). This makes multi-stage amplification difficult in such cases, given that the noise floor of the spectrum will eventually degrade the system performance as it becomes difficult to differentiate between the noise and the signal. These applications also rely on high mutual coherence between comb lines over time, such that pulse to pulse power fluctuations are low, and that power fluctuations on different modes between pulses is essentially zero, although in systems with post-transmission compensation such as in modern optical communications systems, much of these fluctuations may be mitigated.

For optical injection locking, however, the requirements are partially loosened because the slave laser acts not only as a gain medium, but also a filter, and can therefore remove spurious tones and noise outside the locking bandwidth.

CHAPTER 4

Future outlook

In this chapter, a selection of related topics to this thesis are discussed. This discussion does not include OCT, whose applications are readily apparent in the imaging fields, such as the real time imaging of retinas, cardiology, oncology, dermatology, and various nondestructive testing techniques for industrial applications.

Low noise optical tones from a comb source, then, may be used for the following potential applications:

Phase Sensitive Amplification
The primary motivation for producing low noise and highly tunable lasers in our lab is for their use in phase sensitive amplifiers [34], which are useful for low noise regenerative loops, optical communications, and more.

Typically, in order to produce the idler required in PSAs, a copier is used. Here, the pump(s) and signal are launched into some length of nonlinear medium to necessarily produce an idler wave at the required frequnecy. Then, the pump(s) are regenerated via amplification, phases are fixed for maximum gain in the PSA, and the 4 waves pass through a nonlinear medium for power conversion. The role of a low noise highly tunable laser then, would be to replace the copier and therefore remove the need for one of the two lengths of nonlinear medium, as well as the regenerative pump amplifier.

To that end, there are plans in the near to immediate future to replace the copier stage of a PSA with a comb-based tunable source, seeded with a low noise laser.

Optical Communications

In the case of optical communications, using ultra-low noise amplifiers is important for long haul systems where noise buildup due to amplification is often a limiting factor in system throughput [105]. A traditional optical amplifier relies on stimulated emission to produce gain, along with which comes a 3 dB floor due to the amplifier's NF from ASE. To that end, PSAs, which may offer less than 3 dB NF, and are theoretically capable of offering a 0 dB NF, are of interest [106], since they rely on nonlinear power transfer instead of direct emission.

In the proposed scheme for optical communications, a signal is encoded with data, and an idler which has been produced by the low noise tunable laser, is precisely placed in frequency space relative to the signal and pump(s). This idler is then encoded with conjugate data. Over some distance through the nonlinear media, power is transferred from the pump onto the signal and idler, producing low noise amplification. Of course, such a system is useful in that it replaces the copier, but it adds additional complexity by requiring new modulators for data encoding, for instance. Still, in some situations, this trade-off may be beneficial.

Resonant Excitation

Tunable low noise lasers are particularly interesting for their ability to excite specific resonances of a system. This could be a molecular or atomic system, such as a single vibrational mode of a particular atom or molecule, or even an optical system such as a resonant cavity.

One such application of resonant excitation may be atom trapping [107, 108] and cooling [109, 110], whereby a laser with high frequency stability manipulates some atomic material via absorption and reflection. In doing so, the photon's energy / momentum is imparted onto the atom, which can be used to lock it in place, or to effectively cool the material via a specific atomic or ionic transition.

Another common application might be the excitation of optical resonances. The typical pumping instrument for lab use in microresonator frequency combs, for example, is a low noise external cavity laser, but could easily be replaced by a low noise tunable laser such as the one proposed here. Indeed, ECDLs are bulky and rely on high stability of

the external cavity, which makes them difficult to apply in the field. An integrated platform, however, is compact and is necessarily more stable and thus practical in out-of-lab situations.

Metrology

High quality lasers such as the ones produced here are particularly useful when viewed as an absolute frequency reference, such as when calibrating various optical equipment [111], precise measurements of distance such as in LIDAR systems [41, 42], and for precision spectroscopy [112].

Metrology is a wide field with a huge range of applications, but such measurements are particularly useful in defining standards like the length of the meter and the definition of a second.

Of course, having a high precision frequency is also useful for a variety of other tasks, such as when used as a reference to which other lasers may be locked in data communications centers, etc.

CHAPTER 5

Summary of papers

5.1 Summary of Papers

Attached hereafter are the relevant research works:

Paper A
Widely tunable, low linewidth, and high power laser source using an electro-optic comb and injection-locked slave laser array
Optics Express, vol. 29, no. 11, May 2022

This paper covers work done at Chalmers, and focuses on the assembly of a fixed-frequency, low noise laser source which is highly tunable. A low noise seed laser is used to produce an electro-optic (EO) frequency comb via 25 GHz cascaded modulation side bands. After production, a tone is picked off and used for injection locking via an array of distributed feedback (DFB) lasers. By tuning the seed laser across a frequency range greater than the RF clock's oscillation frequency, any frequency of output across the comb's bandwidth is achievable. This work achieves a single frequency tunable laser which has less than 400 Hz of linewidth across its full tunable range of ~ 10 nm, has approximately 55 dB SMSR, and approximately 20 dBm of output power.

Paper B

Widely Tunable and Narrow Linewidth Laser Source based on Normal-Dispersion Frequency Combs and Optical Injection Locking
submitted to *Conference on Lasers and Electro-Optics (CLEO)*, San Jose, USA, May 2022.

This paper also covers work done at Chalmers and can be thought of as a direct follow-up work to [Paper A]. Here, the same low noise seed laser is used to produce a microresonator frequency comb in a normal dispersion photonic molecule, after which individual tones are picked off and injection locked via a single Fabry-Perot (FP) laser. By using a microresonator frequency comb, the free spectral range of comb lines is increased by a factor of 4 (up to 100 GHz), and by using a single FP slave laser, the complexity and footprint of the system is greatly reduced. Moreover, the process is highly efficient in comparison with the previous result. The resulting output laser does incur some penalty in phase/frequency noise and in final output power, but is significantly more tunable - notably, across the full C-Band of operation. It acheives $\sim$ 55 nm of tunable range, over which the SMSR stays above 60 dB, power stays above 5 dBm, and the linewidth stays below 8 kHz.

Paper C
Soliton microcomb based spectral domain optical coherence tomography
Nature Communications, 12:427, 2021.

This work covers work done at EPFL, and focuses on the application of microresonator fequency combs for optical coherence tomography (OCT). My part of this work focused on the relative intensity noise (RIN) measurements for both single soliton and chaotic MI states, as well as the cross correlation measurements between various comb lines. Here, the low noise and high mutual coherence of tones are used for advanced imaging of biological tissue.

References

[1] A. J. Gross and T. R. Herrmann, "History of lasers," *World journal of urology*, vol. 25, no. 3, pp. 217–220, 2007.

[2] Z. Yaqoob and N. A. Riza, "Passive optics no-moving-parts barcode scanners," *IEEE Photonics Technology Letters*, vol. 16, no. 3, pp. 954–956, 2004.

[3] M. Ikeda and S. Uchida, "Blue–violet laser diodes suitable for blu-ray disk," *Physica Status Solidi (a)*, vol. 194, no. 2, pp. 407–413, 2002.

[4] G. P. Agrawal, *Fiber-optic communication systems*. John Wiley & Sons, 2012, vol. 222.

[5] H. J. Eichler, J. Eichler, and O. Lux, *Lasers: basics, advances and applications*. Springer, 2018, vol. 220.

[6] B. P. Abbott, R. Abbott, T. Abbott, M. Abernathy, F. Acernese, K. Ackley, C. Adams, T. Adams, P. Addesso, R. Adhikari *et al.*, "Observation of gravitational waves from a binary black hole merger," *Physical Review Letters*, vol. 116, no. 6, p. 061102, 2016.

[7] J. Ketelaer, J. Krämer, D. Beck, K. Blaum, M. Block, K. Eberhardt, G. Eitel, R. Ferrer, C. Geppert, S. George *et al.*, "TRIGA-SPEC: A setup for mass spectrometry and laser spectroscopy at the research reactor TRIGA mainz," *Nuclear Instruments and Methods in Physics Research Section A: Accelerators, Spectrometers,*

Detectors and Associated Equipment, vol. 594, no. 2, pp. 162–177, 2008.

[8] T. W. Hänsch, "Nobel lecture: passion for precision," *Reviews of Modern Physics*, vol. 78, no. 4, p. 1297, 2006.

[9] T. Udem, R. Holzwarth, and T. W. Hänsch, "Optical frequency metrology," *Nature*, vol. 416, no. 6877, pp. 233–237, 2002.

[10] A. D. Ludlow, M. M. Boyd, J. Ye, E. Peik, and P. O. Schmidt, "Optical atomic clocks," *Reviews of Modern Physics*, vol. 87, no. 2, p. 637, 2015.

[11] P. Delva, J. Lodewyck, S. Bilicki, E. Bookjans, G. Vallet, R. Le Targat, P.-E. Pottie, C. Guerlin, F. Meynadier, C. Le Poncin-Lafitte *et al.*, "Test of special relativity using a fiber network of optical clocks," *Physical Review Letters*, vol. 118, no. 22, p. 221102, 2017.

[12] H. Bergeron, L. C. Sinclair, W. C. Swann, C. W. Nelson, J.-D. Deschênes, E. Baumann, F. R. Giorgetta, I. Coddington, and N. R. Newbury, "Tight real-time synchronization of a microwave clock to an optical clock across a turbulent air path," *Optica*, vol. 3, no. 4, pp. 441–447, 2016.

[13] Y.-S. Jang and S.-W. Kim, "Distance measurements using mode-locked lasers: a review," *Nanomanufacturing and Metrology*, vol. 1, no. 3, pp. 131–147, 2018.

[14] K. Minoshima and H. Matsumoto, "High-accuracy measurement of 240-m distance in an optical tunnel by use of a compact femtosecond laser," *Applied Optics*, vol. 39, no. 30, pp. 5512–5517, 2000.

[15] I. Coddington, W. C. Swann, and N. R. Newbury, "Coherent multiheterodyne spectroscopy using stabilized optical frequency combs," *Physical Review Letters*, vol. 100, no. 1, p. 013902, 2008.

[16] S. A. Diddams, A. Bartels, T. M. Ramond, C. W. Oates, S. Bize, E. A. Curtis, J. C. Bergquist, and L. Hollberg, "Design and control of femtosecond lasers for optical clocks and the synthesis of low-noise optical and microwave signals," *IEEE Journal of Selected Topics in Quantum Electronics*, vol. 9, no. 4, pp. 1072–1080, 2003.

[17] T. Fortier and E. Baumann, "20 years of developments in optical frequency comb technology and applications," *Communications Physics*, vol. 2, no. 1, pp. 1–16, 2019.

[18] R. Holzwarth, M. Zimmermann, T. Udem, and T. Hansch, "Optical clockworks and the measurement of laser frequencies with a mode-locked frequency comb," *IEEE Journal of Quantum Electronics*, vol. 37, no. 12, pp. 1493–1501, 2001.

[19] A. L. Gaeta, M. Lipson, and T. J. Kippenberg, "Photonic-chip-based frequency combs," *Nature Photonics*, vol. 13, no. 3, pp. 158–169, 2019.

[20] P. Del'Haye, A. Schliesser, O. Arcizet, T. Wilken, R. Holzwarth, and T. J. Kippenberg, "Optical frequency comb generation from a monolithic microresonator," *Nature*, vol. 450, no. 7173, pp. 1214–1217, 2007.

[21] A. Parriaux, K. Hammani, and G. Millot, "Electro-optic frequency combs," *Advances in Optics and Photonics*, vol. 12, no. 1, pp. 223–287, 2020.

[22] A. Ruehl, M. J. Martin, K. C. Cossel, L. Chen, H. McKay, B. Thomas, C. Benko, L. Dong, J. M. Dudley, M. E. Fermann *et al.*, "Ultrabroadband coherent supercontinuum frequency comb," *Physical Review A*, vol. 84, no. 1, p. 011806, 2011.

[23] I. Coddington, N. Newbury, and W. Swann, "Dual-comb spectroscopy," *Optica*, vol. 3, no. 4, pp. 414–426, 2016.

[24] N. Li, C. P. Ho, I.-T. Wang, P. Pitchappa, Y. H. Fu, Y. Zhu, and L. Y. T. Lee, "Spectral imaging and spectral lidar systems: moving toward compact nanophotonics-based sensing," *Nanophotonics*, 2021.

[25] J. Liu, E. Lucas, A. S. Raja, J. He, J. Riemensberger, R. N. Wang, M. Karpov, H. Guo, R. Bouchand, and T. J. Kippenberg, "Photonic microwave generation in the x-and k-band using integrated soliton microcombs," *Nature Photonics*, vol. 14, no. 8, pp. 486–491, 2020.

[26] H. Hu, F. Da Ros, M. Pu, F. Ye, K. Ingerslev, E. P. da Silva, M. Nooruzzaman, Y. Amma, Y. Sasaki, T. Mizuno *et al.*, "Single-source chip-based frequency comb enabling extreme parallel data transmission," *Nature Photonics*, vol. 12, no. 8, pp. 469–473, 2018.

[27] H. Al-Taiy, N. Wenzel, S. Preußler, J. Klinger, and T. Schneider, "Ultra-narrow linewidth, stable and tunable laser source for optical communication systems and spectroscopy," *Optics Letters*, vol. 39, no. 20, pp. 5826–5829, 2014.

[28] S. Latkowski, A. Hänsel, P. Van Veldhoven, D. DâAgostino, H. Rabbani-Haghighi, B. Docter, N. Bhattacharya, P. Thijs, H. Ambrosius, M. Smit *et al.*, "Monolithically integrated widely tunable laser source operating at 2 μm," *Optica*, vol. 3, no. 12, pp. 1412–1417, 2016.

[29] Z. Li, S. Alam, Y. Jung, A. Heidt, and D. Richardson, "All-fiber, ultra-wideband tunable laser at 2 μm," *Optics letters*, vol. 38, no. 22, pp. 4739–4742, 2013.

[30] B. Li, W. Jin, L. Wu, L. Chang, H. Wang, B. Shen, Z. Yuan, A. Feshali, M. Paniccia, K. J. Vahala *et al.*, "Reaching fiber-laser coherence in integrated photonics," *Optics Letters*, vol. 46, no. 20, pp. 5201–5204, 2021.

[31] Y. Fan, A. van Rees, P. J. Van der Slot, J. Mak, R. M. Oldenbeuving, M. Hoekman, D. Geskus, C. G. Roeloffzen, and K.-J. Boller, "Hybrid integrated inp-si 3 n 4 diode laser with a 40-hz intrinsic linewidth," *Optics express*, vol. 28, no. 15, pp. 21 713–21 728, 2020.

[32] J. M. Schmitt, "Optical coherence tomography (OCT): a review," *IEEE Journal of Selected Topics in Quantum Electronics*, vol. 5, no. 4, pp. 1205–1215, 1999.

[33] J. F. De Boer, R. Leitgeb, and M. Wojtkowski, "Twenty-five years of optical coherence tomography: the paradigm shift in sensitivity and speed provided by fourier domain oct," *Biomedical optics express*, vol. 8, no. 7, pp. 3248–3280, 2017.

[34] P. A. Andrekson and M. Karlsson, "Fiber-based phase-sensitive optical amplifiers and their applications," *Advances in Optics and Photonics*, vol. 12, no. 2, pp. 367–428, 2020.

[35] W. Demtröder, *Laser spectroscopy: basic concepts and instrumentation*. Springer Science & Business Media, 2013.

[36] M. Françon, "Optical interferometry," in *Neutron interferometry*, 1979.

[37] M.-A. Beeck and W. Hentschel, "Laser metrology â a diagnostic tool in automotive development processes," *Optics and Lasers in Engineering*, vol. 34, no. 2, pp. 101–120, 2000.

[38] D. O. Caplan, "Laser communication transmitter and receiver design," in *Free-Space Laser Communications*. Springer, 2007, pp. 109–246.

[39] J. R. Moffitt, Y. R. Chemla, S. B. Smith, and C. Bustamante, "Recent advances in optical tweezers," *Annu. Rev. Biochem.*, vol. 77, pp. 205–228, 2008.

[40] M. Jaboyedoff, T. Oppikofer, A. Abellán, M.-H. Derron, A. Loye, R. Metzger, and A. Pedrazzini, "Use of lidar in landslide investigations: a review," *Natural hazards*, vol. 61, no. 1, pp. 5–28, 2012.

[41] M. A. Wulder, J. C. White, R. F. Nelson, E. Næsset, H. O. Ørka, N. C. Coops, T. Hilker, C. W. Bater, and T. Gobakken, "Lidar sampling for large-area forest characterization: A review," *Remote Sensing of Environment*, vol. 121, pp. 196–209, 2012.

[42] J. S. Deems, T. H. Painter, and D. C. Finnegan, "Lidar measurement of snow depth: a review," *Journal of Glaciology*, vol. 59, no. 215, pp. 467–479, 2013.

[43] E. D. Kaplan and C. Hegarty, *Understanding GPS/GNSS: principles and applications*. Artech house, 2017.

[44] R. Stolen, "Fiber raman lasers," in *Fiber and Integrated Optics*. Springer, 1979, pp. 157–182.

[45] J. A. Piper and H. M. Pask, "Crystalline raman lasers," *IEEE Journal of Selected Topics in Quantum Electronics*, vol. 13, no. 3, pp. 692–704, 2007.

[46] H. M. Pask, "The design and operation of solid-state raman lasers," *Progress in Quantum Electronics*, vol. 27, no. 1, pp. 3–56, 2003.

[47] K. Hill, B. Kawasaki, and D. Johnson, "Cw brillouin laser," *Applied Physics Letters*, vol. 28, no. 10, pp. 608–609, 1976.

[48] G. Valley, "A review of stimulated brillouin scattering excited with a broad-band pump laser," *IEEE Journal of Quantum Electronics*, vol. 22, no. 5, pp. 704–712, 1986.

[49] E. Garmire, "Stimulated brillouin review: invented 50 years ago and applied today," *International Journal of Optics*, vol. 2018, 2018.

[50] X. Ji, X. Yao, A. Klenner, Y. Gan, A. L. Gaeta, C. P. Hendon, and M. Lipson, "Chip-based frequency comb sources for optical coherence tomography," *Optics express*, vol. 27, no. 14, pp. 19 896–19 905, 2019.

[51] T. Bajraszewski, M. Wojtkowski, M. Szkulmowski, A. Szkulmowska, R. Huber, and A. Kowalczyk, "Improved spectral optical coherence tomography using optical frequency comb," *Optics express*, vol. 16, no. 6, pp. 4163–4176, 2008.

[52] S.-J. Lee, B. Widiyatmoko, M. Kourogi, and M. Ohtsu, "Ultrahigh scanning speed optical coherence tomography using optical frequency comb generators," *Japanese Journal of Applied Physics*, vol. 40, no. 8B, p. L878, 2001.

[53] Y. K. Chembo, "Kerr optical frequency combs: theory, applications and perspectives," *Nanophotonics*, vol. 5, no. 2, pp. 214–230, 2016.

[54] S. A. Diddams, K. Vahala, and T. Udem, "Optical frequency combs: coherently uniting the electromagnetic spectrum," *Science*, vol. 369, no. 6501, 2020.

[55] J. Li, Y. Qu, R. Yu, and Y. Wu, "Generation and control of optical frequency combs using cavity electromagnetically induced transparency," *Physical Review A*, vol. 97, no. 2, p. 023826, 2018.

[56] T. Tanabe, S. Fujii, and R. Suzuki, "Review on microresonator frequency combs," *Japanese Journal of Applied Physics*, vol. 58, no. SJ, p. SJ0801, 2019.

[57] T. Udem and F. Riehle, "Frequency combs applications and optical frequency standards," *La Rivista del Nuovo Cimento*, vol. 30, no. 12, pp. 563–606, 2007.

[58] T. Udem, R. Holzwarth, and T. Hänsch, "Femtosecond optical frequency combs," *The European Physical Journal Special Topics*, vol. 172, no. 1, pp. 69–79, 2009.

[59] M. Zajnulina, J. C. Boggio, M. Böhm, A. A. Rieznik, T. Fremberg, R. Haynes, and M. Roth, "Generation of optical frequency combs via four-wave mixing processes for low-and medium-resolution astronomy," *Applied Physics B*, vol. 120, no. 1, pp. 171–184, 2015.

[60] A. Rueda, F. Sedlmeir, M. Kumari, G. Leuchs, and H. G. Schwefel, "Resonant electro-optic frequency comb," *Nature*, vol. 568, no. 7752, pp. 378–381, 2019.

[61] L. Lugiato, F. Prati, M. Gorodetsky, and T. Kippenberg, "From the lugiato–lefever equation to microresonator-based soliton Kerr frequency combs," *Philosophical Transactions of the Royal Society A: Mathematical, Physical and Engineering Sciences*, vol. 376, no. 2135, p. 20180113, 2018.

[62] T. Herr, K. Hartinger, J. Riemensberger, C. Wang, E. Gavartin, R. Holzwarth, M. Gorodetsky, and T. Kippenberg, "Universal formation dynamics and noise of Kerr-frequency combs in microresonators," *Nature Photonics*, vol. 6, no. 7, pp. 480–487, 2012.

[63] A. Coillet and Y. K. Chembo, "Routes to spatiotemporal chaos in Kerr optical frequency combs," *Chaos: An Interdisciplinary Journal of Nonlinear Science*, vol. 24, no. 1, p. 013113, 2014.

[64] Z. Kang, F. Li, J. Yuan, K. Nakkeeran, J. N. Kutz, Q. Wu, C. Yu, and P. Wai, "Deterministic generation of single soliton Kerr frequency comb in microresonators by a single shot pulsed trigger," *Optics express*, vol. 26, no. 14, pp. 18 563–18 577, 2018.

[65] T. J. Kippenberg, A. L. Gaeta, M. Lipson, and M. L. Gorodetsky, "Dissipative Kerr solitons in optical microresonators," *Science*, vol. 361, no. 6402, 2018.

[66] D. C. Cole, E. S. Lamb, P. Del'Haye, S. A. Diddams, and S. B. Papp, "Soliton crystals in Kerr resonators," *Nature Photonics*, vol. 11, no. 10, pp. 671–676, 2017.

[67] M. Karpov, M. H. Pfeiffer, H. Guo, W. Weng, J. Liu, and T. J. Kippenberg, "Dynamics of soliton crystals in optical microresonators," *Nature Physics*, vol. 15, no. 10, pp. 1071–1077, 2019.

[68] Y. He, J. Ling, M. Li, and Q. Lin, "Perfect soliton crystals on demand," *Laser & Photonics Reviews*, vol. 14, no. 8, p. 1900339, 2020.

[69] E. Lucas, M. Karpov, H. Guo, M. Gorodetsky, and T. J. Kippenberg, "Breathing dissipative solitons in optical microresonators," *Nature communications*, vol. 8, no. 1, pp. 1–11, 2017.

[70] H. Guo, E. Lucas, M. H. Pfeiffer, M. Karpov, M. Anderson, J. Liu, M. Geiselmann, J. D. Jost, and T. J. Kippenberg, "Intermode breather solitons in optical microresonators," *Physical Review X*, vol. 7, no. 4, p. 041055, 2017.

[71] J. Riemensberger, K. Hartinger, T. Herr, V. Brasch, R. Holzwarth, and T. J. Kippenberg, "Dispersion engineering of thick high-q silicon nitride ring-resonators via atomic layer deposition," *Optics express*, vol. 20, no. 25, pp. 27 661–27 669, 2012.

[72] Ó. B. Helgason, F. R. Arteaga-Sierra, Z. Ye, K. Twayana, P. A. Andrekson, M. Karlsson, J. Schröder, and V. Torres-Company, "Dissipative solitons in photonic molecules," *Nature Photonics*, vol. 15, no. 4, pp. 305–310, 2021.

[73] A. Tikan, J. Riemensberger, K. Komagata, S. Hönl, M. Churaev, C. Skehan, H. Guo, R. N. Wang, J. Liu, P. Seidler *et al.*, "Emergent nonlinear phenomena in a driven dissipative photonic dimer," *Nature Physics*, vol. 17, no. 5, pp. 604–610, 2021.

[74] A. E. Siegman, "Lasers university science books," *Mill Valley, CA*, vol. 37, no. 208, p. 169, 1986.

[75] O. Svelto and D. C. Hanna, *Principles of lasers*. Springer, 1998, vol. 4.

[76] I. Joindot, "Measurements of relative intensity noise (rin) in semiconductor lasers," *Journal de Physique III*, vol. 2, no. 9, pp. 1591–1603, 1992.

[77] C. W. Nelson, A. Hati, and D. A. Howe, "Relative intensity noise suppression for RF photonic links," *IEEE Photonics Technology Letters*, vol. 20, no. 18, pp. 1542–1544, 2008.

[78] M. Huber, W. Schweinberger, F. Stutzki, J. Limpert, I. Pupeza, and O. Pronin, "Active intensity noise suppression for a broadband mid-infrared laser source," *Optics express*, vol. 25, no. 19, pp. 22 499–22 509, 2017.

[79] G. E. Obarski, P. D. Hale *et al.*, "How to measure relative intensity noise in lasers," *Laser Focus World*, vol. 35, pp. 273–278, 1999.

[80] G. Di Domenico, S. Schilt, and P. Thomann, "Simple approach to the relation between laser frequency noise and laser line shape," *Applied optics*, vol. 49, no. 25, pp. 4801–4807, 2010.

[81] A. L. Schawlow and C. H. Townes, "Infrared and optical masers," *Phys. Rev.*, vol. 112, pp. 1940–1949, Dec 1958. [Online]. Available: https://link.aps.org/doi/10.1103/PhysRev.112.1940

[82] C. Henry, "Theory of the linewidth of semiconductor lasers," *IEEE Journal of Quantum Electronics*, vol. 18, no. 2, pp. 259–264, 1982.

[83] P. Goldberg, P. W. Milonni, and B. Sundaram, "Theory of the fundamental laser linewidth," *Physical Review A*, vol. 44, no. 3, p. 1969, 1991.

[84] M. Ohtsu, K. Nakagawa, M. Kourogi, and W. Wang, "Frequency control of semiconductor lasers," *Journal of applied physics*, vol. 73, no. 12, pp. R1–R17, 1993.

[85] M. A. Tran, D. Huang, and J. E. Bowers, "Tutorial on narrow linewidth tunable semiconductor lasers using si/iii-v heterogeneous integration," *APL photonics*, vol. 4, no. 11, p. 111101, 2019.

[86] S. Camatel and V. Ferrero, "Narrow linewidth cw laser phase noise characterization methods for coherent transmission system applications," *Journal of Lightwave Technology*, vol. 26, no. 17, pp. 3048–3055, 2008.

[87] N. Satyan, J. B. Sendowski, A. Vasilyev, G. A. Rakuljic, and A. Yariv, "Phase noise reduction of a semiconductor laser in a composite optical phase-locked loop," *Optical Engineering*, vol. 49, no. 12, p. 124301, 2010.

[88] D. Arsenijević, M. Kleinert, and D. Bimberg, "Phase noise and jitter reduction by optical feedback on passively mode-locked

quantum-dot lasers," *Applied Physics Letters*, vol. 103, no. 23, p. 231101, 2013.

[89] C. McNeilage, E. Ivanov, P. Stockwell, and J. Searls, "Review of feedback and feedforward noise reduction techniques," in *Proceedings of the 1998 IEEE International Frequency Control Symposium (Cat. No. 98CH36165)*. IEEE, 1998, pp. 146–155.

[90] F. Aflatouni, M. Bagheri, and H. Hashemi, "Design methodology and architectures to reduce the semiconductor laser phase noise using electrical feedforward schemes," *IEEE transactions on microwave theory and techniques*, vol. 58, no. 11, pp. 3290–3303, 2010.

[91] X. Xie, R. Bouchand, D. Nicolodi, M. Lours, C. Alexandre, and Y. Le Coq, "Phase noise characterization of sub-hertz linewidth lasers via digital cross correlation," *Optics letters*, vol. 42, no. 7, pp. 1217–1220, 2017.

[92] L. Richter, H. Mandelberg, M. Kruger, and P. McGrath, "Linewidth determination from self-heterodyne measurements with subcoherence delay times," *IEEE Journal of Quantum Electronics*, vol. 22, no. 11, pp. 2070–2074, 1986.

[93] O. Llopis, P.-H. Merrer, H. Brahimi, K. Saleh, and P. Lacroix, "Phase noise measurement of a narrow linewidth cw laser using delay line approaches," *Optics letters*, vol. 36, no. 14, pp. 2713–2715, 2011.

[94] M. Xue and J. Zhao, "Laser linewidth measurement based on long and short delay fiber combination," *Optics Express*, vol. 29, no. 17, pp. 27 118–27 126, 2021.

[95] S. Huang, T. Zhu, Z. Cao, M. Liu, M. Deng, J. Liu, and X. Li, "Laser linewidth measurement based on amplitude difference comparison of coherent envelope," *IEEE Photonics Technology Letters*, vol. 28, no. 7, pp. 759–762, 2016.

[96] Z. Wang, C. Ke, Y. Zhong, C. Xing, H. Wang, K. Yang, S. Cui, and D. Liu, "Ultra-narrow-linewidth measurement utilizing dual-parameter acquisition through a partially coherent light interference," *Optics express*, vol. 28, no. 6, pp. 8484–8493, 2020.

[97] A. Bordonalli, C. Walton, and A. Seeds, "High performance phase-locking of wide linewidth semiconductor lasers by optical injection phase-lock loop," in *Proceedings of European Conference on Optical Communication*, vol. 2, 1996, pp. 309–312 vol.2.

[98] A. Murakami, K. Kawashima, and K. Atsuki, "Cavity resonance shift and bandwidth enhancement in semiconductor lasers with strong light injection," *IEEE Journal of Quantum Electronics*, vol. 39, no. 10, pp. 1196–1204, 2003.

[99] Z. Liu and R. Slavík, "Optical injection locking: From principle to applications," *Journal of Lightwave Technology*, vol. 38, no. 1, pp. 43–59, 2020.

[100] F. Mogensen, H. Olesen, and G. Jacobsen, "Locking conditions and stability properties for a semiconductor laser with external light injection," *IEEE Journal of Quantum Electronics*, vol. 21, no. 7, pp. 784–793, 1985.

[101] N. R. Newbury and W. C. Swann, "Low-noise fiber-laser frequency combs," *JOSA B*, vol. 24, no. 8, pp. 1756–1770, 2007.

[102] R. Paschotta, A. Schlatter, S. Zeller, H. Telle, and U. Keller, "Optical phase noise and carrier-envelope offset noise of mode-locked lasers," *Applied Physics B*, vol. 82, no. 2, pp. 265–273, 2006.

[103] H. R. Telle, B. Lipphardt, and J. Stenger, "Kerr-lens, mode-locked lasers as transfer oscillators for optical frequency measurements," *Applied Physics B*, vol. 74, no. 1, pp. 1–6, 2002.

[104] J. Stenger, H. Schnatz, C. Tamm, and H. R. Telle, "Ultraprecise measurement of optical frequency ratios," *Physical Review Letters*, vol. 88, no. 7, p. 073601, 2002.

[105] A. Bononi, J.-C. Antona, and P. Serena, "The generalized droop model for optical long-haul transmission systems." in *ECOC*, 2020, pp. 1–4.

[106] S. L. Olsson, H. Eliasson, E. Astra, M. Karlsson, and P. A. Andrekson, "Long-haul optical transmission link using low-noise phase-sensitive amplifiers," *Nature communications*, vol. 9, no. 1, pp. 1–7, 2018.

[107] C. Bradac, "Nanoscale optical trapping: a review," *Advanced Optical Materials*, vol. 6, no. 12, p. 1800005, 2018.

[108] M. Tomza, K. Jachymski, R. Gerritsma, A. Negretti, T. Calarco, Z. Idziaszek, and P. S. Julienne, "Cold hybrid ion-atom systems," *Reviews of modern physics*, vol. 91, no. 3, p. 035001, 2019.

[109] B. Zhao, M. Hu, X. Ao, N. Chen, and G. Pei, "Radiative cooling: A review of fundamentals, materials, applications, and prospects," *Applied energy*, vol. 236, pp. 489–513, 2019.

[110] L. Anderegg, B. L. Augenbraun, Y. Bao, S. Burchesky, L. W. Cheuk, W. Ketterle, and J. M. Doyle, "Laser cooling of optically trapped molecules," *Nature Physics*, vol. 14, no. 9, pp. 890–893, 2018.

[111] E. Goetz and R. Savage, "Calibration of the ligo displacement actuators via laser frequency modulation," *Classical and Quantum Gravity*, vol. 27, no. 21, p. 215001, 2010.

[112] W. Majewski, "A tunable, single frequency uv source for high resolution spectroscopy in the 293–330 nm range," *Optics Communications*, vol. 45, no. 3, pp. 201–206, 1983.

Included papers A–C

Paper A

"Widely tunable, low linewidth, and high power lasers source using an electro-optic comb and injeciton-locked slave laser array",
J. Connor Skehan, Corentin Naveau, Jochen Schröder, and Peter Andrekson
Optics Express, vol. 29, no. 11, May 2022

Paper B

"Widely Tunable and Narrow Linewidth Laser Sourced based on Normal-Dispersion Frequency Combs and Optical Injection Locking",
J. Connor Skehan, Oskar B. Helgason, Jochen Schröder, Victor Torres-Company, and Peter Andrekson
submitted to *Conference on Lasers and Electro-Optics (CLEO)*, San Jose, USA, May 2022.

Paper C

"Soliton microcomb based spectral domain optical coherence tomography",
Paul J. Marchand, Johann Riemensberger, **J. Connor Skehan**, Jia-Jung Ho, Martin H. P. Pfeiffer, Junqiu Liu, Christoph Hauger, Theo Lasser, Tobias J. Kippenberg
Nature Communications, 12:427, 2021.